Journal of Applied Fluid Mechanics, Vol. 14, No. 2, pp. 459-472, 2021.
Available online at www.jafmonline.net, ISSN 1735-3572, EISSN 1735-3645.
DOI: 10.47176/jafm.14.02.31381

Natural Convection of Power Law Fluid through a Porous Deposit: MRT-LBM Approach

A. Bourada[1†], A. Boutra[1, 2], K. Bouarnouna[1], D. E. Ameziani[3] and Y. K. Benkahla[1]

[1] *Laboratory of Transfer Phenomena, RSNE Team, FGMGP, USTHB, Bab Ezzouar, Algiers, 16111, Algeria*
[2] *Superior School of Applied Sciences, Casbah, Algiers,16001, Algeria*
[3] *Laboratory of Multiphase Transport and Porous Media, FGMGP, USTHB, Bab Ezzouar, Algiers, 16111, Algeria*

†*Corresponding Author Email: abderrahmanebourada@gmail.com*

(Received January 23, 2020; accepted July 25, 2020)

ABSTRACT

In this research, natural convection of power law fluid in a square cavity, with a porous deposit in the shape of a semi-cylinder is studied numerically, using the multiple-relaxation-time lattice Boltzmann method. The modified Darcy-Brinkman model is applied for modelling the momentum equations in porous medium and the Boussinesq assumption is adopted to model the buoyancy force term. The influences of power law index ($0.6 \le n \le 1.4$), Darcy number ($10^{-5} \le Da \le 10^{-2}$), Rayleigh number ($10^3 \le Ra \le 10^6$) and the radius ratio of the semi-cylindrical porous deposit ($0.05 \le R \le 0.5$) on hydrodynamic and heat transfer are studied. The obtained results show that these parameters have an important effect, on the structure of hydrodynamic and thermal transfer. The improvement of the power law index leads to a decrease in the heat transfer rate, illustrated by the average Nusselt number, and the augmentation in Darcy number induces an increase in that rate. Moreover, the variation of the Rayleigh number and the porous deposit radius has a significant effect on the transfer rate and convective structure. Besides, an unusual phenomenon is noticed for high Rayleigh numbers, where a better heat evacuation from the porous deposit is noticed for the dilatant fluid compared to the pseudoplastic one.

Keywords: Modified Darcy-Brinkman model; Square cavity; Semi-cylinder.

NOMENCLATURE

Ct	tortuosity factor
c_p	specific heat of fluid
Da	Darcy number
e_i	discrete particle velocity
F	total body force
f_i	density distribution function
G	driving force
g	acceleration of gravity
K	permeability of the porous medium
k	thermal conductivity
K^*	modified permeability of the porous medium
K'	consistency coefficient
L	length and height of the cavity
LBM	Lattice Boltzmann Method
MRT	Multiple-Relaxation-Time
n	power law index
n′	modified power law index
Nu	local Nusselt number
Nu_{avg}	average Nusselt number
p	pressure
Pr	Prandtl number
$\dot{\gamma}$	local shear rate
ε	porosity of porous medium
θ	dimensionless temperature
μ_a	apparent dynamic viscosity
ρ	fluid density
σ	porous matrix coefficient
υ	kinematic viscosity
υ_e	effective kinematic viscosity
R	dimensionless radius of porous deposit
r	dimensional radius of porous deposit
Ra	Rayleigh number
s_i	relaxation rate
$S_{\alpha'\beta'}$	strain rate tensor
T	temperature
t	time
v_x	dimensional velocity component in x-direction
v_y	dimensional velocity component in y-direction
V_x	dimensionless velocity component in x-direction
V_y	dimensionless velocity component in y-direction
w	size of heat source

x, y	dimensional Cartesian coordinates
X, Y	dimensionless Cartesian coordinates
α	thermal conductivity
β	thermal expansion coefficient
α', β'	cartesian coordinates
Ω	collision operator

Subscripts

avg	average
C	cold
e	effective
eq	equilibrium
H	hot
i	direction index

1. INTRODUCTION

The problem of natural convection in a medium with porous matrix has attracted the attention of numerous researchers, due to the wide range of relevant applications in mechanical, technical and chemical fields, such as electronic cooling, fibrous insulation, packed-bed reactors, fluid flow in geothermal reservoirs, crude oil production, grain storage system, food processing, drying,…etc.

Over the last few decades, the free convection of Newtonian fluids in porous medium has been considered by many authors. Basak *et al.* (2006) have compared, in natural convection, the impact of uniform versus non-uniform heating, in an entirely porous square cavity, employing the Darcy-Forchheimer model. Jafari *et al.* (2018) considered natural convection of nanofluid for five different configurations of square porous cavities, equipped with cylindrical hot pins, using the lattice Boltzmann method. Ragui *et al.* (2017) have simulated free convection in a partitioned porous cavity, under the effect of thermosolutal buoyancy forces. Habbachi *et al.* (2017) have examined heat transfer in natural convection inside cubic enclosure, equipped with a cubic porous obstacle. Numerical investigation on the influence of porous layer thickness was proposed by Chen *et al.* (2009). Heidary *et al.* (2016) analysed natural convection in porous inclined enclosures, equipped with one or two obstacles, with the presence of sinusoidal heated wall and magnetic field. A numerical investigation on natural convection was performed by Astanina *et al.* (2018) in a partially porous square cavity. The latter contains a conductive and heat-generating block. The simulations were run using Darcy-Brinkman equation and considering a temperature-dependent viscosity. Omara *et al.* (2016) performed a numerical study on natural convection in a square porous enclosure with partially heated left wall and partially cooled right one. The study was realized using thermal non equilibrium model and Darcy-Brinkman-Forchheimer equation.

The investigation of the natural convection of Newtonian and power law fluids also attracted considerable attention in recent decades. Dash *et al.* (2014) introduced a novel flexible forcing immersed boundary LBM for simulating natural convection in an annulus of hot eccentric square inner cylinder. Habibi Matin *et al.* (2013) have simulated the natural convection of power law fluid in an annulus. Turan *et al.* (2011) studied numerically the free convection in differentially heated cavities, saturated by power law fluids. Gangawane and Manikandan (2017) have compared, in natural convection, the isothermal heating to the uniform heat flow of a hexagonal block attached to the centre of a square enclosure. The latter is filled with power law fluid. Dash and lee (2014) used a new flexible forcing immersed boundary LBM to study numerically the natural convection in an enclosure, equipped with inclined square hot cylinder. Moreover, Dash and Lee (2015) studied free convection within a square enclosure with different horizontal and diagonal eccentric square heat sources. Khezzar *et al.* (2012) have treated natural convection in inclined cavities, saturated by power law fluids, for various aspect ratios.

Nevertheless, natural convection of Ostwald-de Waele fluids in porous media has not been treated considerably. Jecl and Skerget (2003) have presented free convection in totally porous square enclosures, containing power law and Carreau fluids. The work was done using the modified Darcy-Brinkman model for flow in porous medium and considering the non-Darcy viscous effects. Abdel-gaied and Eid (2011) have performed a study of thermosolutal natural convection of Ostwald-de Waele fluids, flowing on an axisymmetric body of arbitrary form in a porous media. The work was done utilizing the modified Darcy model. In natural convection mode, Getachew *et al.* (1996) have used the modified Darcy equation to model the power law fluid flow in a porous cavity. Kefayati (2016) used finite difference LBM to simulate thermosolutal natural convection of Ostwald-de Waele fluids within inclined porous enclosure. Zhuang *et al.* (2017) have reported a numerical study on thermosolutal natural convection of power law fluids within a porous cubic enclosure by adopting the generalized non-Darcy model and considering a chemical reaction. Zhuang and Zhu (2018) have investigated the buoyancy-Marangoni convection of power law nanofluids saturated porous cubic enclosure by adopting the Darcy-Brinkman model. Raizah Abdelraheem *et al.* (2018) have presented a numerical investigation of laminar flow of power law nanofluid, saturated porous media, inside an inclined open shallow enclosure, where the Darcy model is applied.

Lattice Boltzmann is a relatively new method compared to conventional approaches in numerical simulation. Yet, between the foundation of statistical physics, on which LBM is based, and its theoretical completion, more than a century has passed. The construction of the lattice Boltzmann method can be summarized in two paradoxically independent steps: the development of statistical physics of one side, and the appearance of cellular automatons on the other side. LBM is one of the most powerful and most used approaches for the simulation of transfer phenomena within a porous medium. This may be relative to its simplicity and its ability to manage complex geometries and boundary conditions. This tool has also been used as a computational approach to simulate flows of non-Newtonian fluids.

The scarcity of published works treating the natural convection of non-Newtonian power law fluid in medium with a porous matrix has motivated us to continue in this field. Such fluid flows are abundant in many applications both technologically and theoretically. In this article, the MRT-LBM is developed to solve the general equations governing the convective heat transfer of power law fluid in a square cavity containing a semi-cylindrical porous deposit. The main aim of this study is to determine the combined effect produced by the coexistence of power law fluid and porous matrix, on the hydrodynamic and heat transfer characteristics. This effect was computed by implementing the modified Darcy-Brinkman model for power law fluid in the Boltzmann equation. The influence of diverse parameters such as power law index, Darcy number, Rayleigh number and radius ratio of the semi-cylindrical porous deposit were studied.

2. PHYSICAL PROBLEM

Two-dimensional natural convection of power law fluid is studied in a partially heated square enclosure (Fig. 1). The hot source of size w (w / L = 0.6), is placed at the central part of the bottom wall, and kept at a uniform temperature (T_H). The side walls are maintained at a constant cold temperature (T_C), while the other walls are adiabatic. The cavity contains a semi-cylindrical porous deposit of radius r and constant porosity ε = 0.6, located on the centre of the bottom wall. The porous matrix is considered as homogeneous and isotropic. Also, the fluid and the porous matrix are thermally in equilibrium. We have taken advantage of the modified Darcy-Brinkman model for modelling the momentum equations in the porous deposit.

The fluid is considered as incompressible with constant thermo-physical properties. Only in the buoyancy term, the density is described by the Boussinesq approximation (Bejan 2004). The fluid viscosity is equivalent to the effective viscosity and the Prandtl number is equal to 10 in all the study.

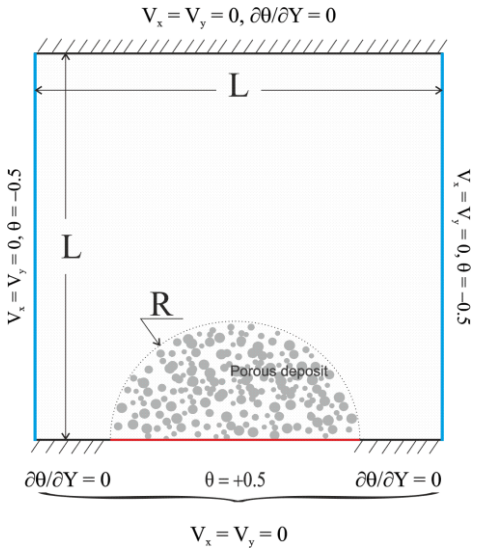

Fig. 1. Physical problem scheme with boundary conditions.

3. MACROSCOPIC GOVERNING EQUATIONS

Based on the assumptions mentioned above: the governing equations of heat transfer by convection in their dimensional form, using momentum and energy conservation, are written, in porous medium and fluid region, as follows (Nebbali and Bouhadef 2011, Shenoy 1994):

Continuity equation

$$\frac{\partial v_x}{\partial x} + \frac{\partial v_y}{\partial y} = 0 \tag{1}$$

x momentum equation:

$$\frac{\partial v_x}{\partial t} + \frac{v_x}{\varepsilon}\frac{\partial v_x}{\partial x} + \frac{v_y}{\varepsilon}\frac{\partial v_x}{\partial y} = -\frac{\varepsilon}{\rho_0}\frac{\partial p}{\partial x} + \frac{\upsilon_e}{\varepsilon^{n-1}}\left(\frac{\partial^2 v_x}{\partial x^2} + \frac{\partial^2 v_x}{\partial y^2}\right) + F_x \tag{2}$$

y momentum equation:

$$\frac{\partial v_y}{\partial t} + \frac{v_x}{\varepsilon}\frac{\partial v_y}{\partial x} + \frac{v_y}{\varepsilon}\frac{\partial v_y}{\partial y} = -\frac{\varepsilon}{\rho_0}\frac{\partial p}{\partial y} + \frac{\upsilon_e}{\varepsilon^{n-1}}\left(\frac{\partial^2 v_y}{\partial x^2} + \frac{\partial^2 v_y}{\partial y^2}\right) + F_y \tag{3}$$

Energy equation:

In the fluid region:

$$\rho c_p\left(\frac{\partial T}{\partial t} + v_x\frac{\partial T}{\partial x} + v_y\frac{\partial T}{\partial y}\right) = k\left(\frac{\partial^2 T}{\partial x^2} + \frac{\partial^2 T}{\partial y^2}\right) \tag{4}$$

In the porous medium:

$$\rho c_p\left(\xi\frac{\partial T}{\partial t}+v_x\frac{\partial T}{\partial x}+v_y\frac{\partial T}{\partial y}\right)=k_e\left(\frac{\partial^2 T}{\partial x^2}+\frac{\partial^2 T}{\partial y^2}\right) \quad (5)$$

where v_x and v_y are respectively the transversal and longitudinal constituents of the averaged volume velocity, ρ_0 is the average fluid density, p the pressure and T the temperature, ε is the porosity of the porous deposit (this parameter is equal to unity in the fluid region), υ_e is the effective kinematic viscosity, $\xi = [\varepsilon(\rho c_p)+(1-\varepsilon)(\rho_s c_{ps})] / (\rho c_p)$ is the ratio of thermal capacity, ρ and ρ_s are densities of the fluid and the solid, respectively, c_p and c_{ps} are respectively the fluid and solid specific heat capacities, k and k_e are the thermal conductivities of the fluid and the porous matrix, respectively. In momentum equations, n is the power law index, $F = (F_x, F_y)$ refers to the body's total force, caused by the existence of the porous deposit, and the Buoyancy term, given by (Nebbali and Bouhadef 2011, Shenoy 1994):

$$F=-\sigma\frac{\varepsilon\upsilon_e}{K^*}|v|^{n-1}v+\varepsilon G \quad (6)$$

where $v = (v_x, v_y)$ is the velocity in the x and y directions, $|v|=\sqrt{v_x^2+v_y^2}$, σ is the porous matrix coefficient which is equal to 1 in the porous region and 0 in the fluid region.

K^* is the modified permeability of Ostwald-de Waele fluid, defined by Christopher and middleman (1965), it relies both on the power law index and the existence of porous medium:

$$K^*=\frac{1}{2C_t}\left(\frac{n\varepsilon}{3n+1}\right)^n\left(\frac{50K}{3\varepsilon}\right)^{(n+1)/2} \quad (7)$$

K refers to the intrinsic permeability and C_t is the tortuosity factor defined thus:

$$C_t=\begin{cases}\dfrac{25}{12} & \text{Christofer and Middelman (1965)}\\ \left(\dfrac{5}{2}\right)^n 2^{(1-n)/2} & \text{Kemblowski and Michiewicz (1979)}\\ \dfrac{2}{3}\left(\dfrac{8n'}{9n'+3}\right)^{n'}\left(\dfrac{10n'-3}{6n'+1}\right)\left(\dfrac{75}{16}\right)^{\frac{3(10n'-3)}{(10n'+1)}} & \text{Dharmadhikari and Kale (1985)}\end{cases} \quad (8)$$

In this work, the Dharmadhikari and Kale (1985) expression is used. For this expression, the power law index must be changed to a new power index:

$n' = n + 0.3(1–n)$.

The driving force G described by the Boussinesq approximation is given by:

$$G=-g\beta(T-T_0)j \quad (9)$$

in which g is the gravity acceleration, β is the thermal expansion coefficient, $T_0 = (T_H + T_C)/2$ is the reference temperature, j is the unit vector in the y direction.

The shear stress for a power law fluid is depicted in tensor form as (Habibi Matin *et al.* 2013):

$$\tau_{xy}=\mu_a\left(\frac{\partial v_x}{\partial y}+\frac{\partial v_y}{\partial x}\right) \quad (10)$$

μ_a is the apparent viscosity defined by:

$$\mu_a=K'\left\{2\left[\left(\frac{\partial v_x}{\partial x}\right)^2+\left(\frac{\partial v_y}{\partial y}\right)^2\right]+\left(\frac{\partial v_y}{\partial x}+\frac{\partial v_x}{\partial y}\right)^2\right\}^{\frac{n-1}{2}} \quad (11)$$

where K' is the consistency coefficient.

The non-dimensional parameters of this study are:

$$X=\frac{x}{L};Y=\frac{y}{L};V_x=\frac{v_x L}{\alpha_e};V_y=\frac{v_y L}{\alpha_e};Ra=\frac{g\beta(T_H-T_C)L^3}{\upsilon\alpha_e};$$

$$Da=\frac{K^*}{L^2};\Pr=\frac{\upsilon}{\alpha_e};J=\frac{\upsilon_e}{\upsilon};\theta=\frac{T-T_0}{T_H-T_C};R=\frac{r}{L}$$

In which α_e is the effective thermal diffusivity, Ra is the Rayleigh number, Da is the number of Darcy, Pr is the number of Prandtl, L is the characteristic length, υ is the fluid kinetic viscosity, J is the viscosity ratio and R is the radius ratio of the semi-cylindrical porous deposit.

4. LATTICE BOLTZMANN APPROACH

The LBM may be applied to solve the problems of fluid flow, heat transfer and mass transport phenomena. In this approach, the fluid is considered as a set of particles, which move (stream) with discrete velocity in specified directions, depending on the lattice structure, and collide (interact) with each other on lattice nodes. The distribution function f is the probability of finding a particle at a given node with a certain velocity. Collision and particle advection are driven by the LB equation, which reflects the development of these functions and external forces introduced by a source term (Boutra *et al.* 2017, Kumar *et al.* 2017, Shah *et al.* 2017, Sullivan *et al.* 2006):

$$f_i(x+e_i\delta_t,t+\delta_t)-f_i(x,t)=\Omega(f_i)+\delta_t F_i \quad (12)$$

where f_i is the function of distribution with velocity e_i at lattice node x at time t, δ_t is the discrete time step, $\Omega(f_i)$ is the discrete collision operator and F_i is the external forces term.

The lattice Bhatnagar-Gross-Krook (BGK) is the most simple of the LB methods, approximating the collision operator with single relaxation time (Bhatnagar *et al.* 1954, Khali *et al.* 2013). By adopting this approximation, the collision operator is linearized around an f_i^{eq} equilibrium state ; it is thus written in the following matrix form:

$$f_i(x+e_i\delta_t,t+\delta_t)-f_i(x,t)=-\frac{1}{\tau}\left[f_i(x,t)-f_i^{eq}(x,t)\right]+\delta_t F_i \quad (13)$$

where f_i^{eq} is the equilibrium distribution function

and τ is the dimensionless relaxation time.

Numerical instability, limitation in representation of certain flow problems and fixing of Prandtl number and the report of kinematic viscosity to apparent viscosity at the unit values, appear as default of this method and give limits to its use.
In order to overcome these shortcomings, d'Humières (1992) proposed the moment approach known as the multiple-relaxation-time model, employing different relaxation times to simulate the evolution of macroscopic quantities. The execution of the collision in an orthogonal moment space leads to an efficient and flexible scheme. This model presents an optimal stability compared to the BGK model. In the MRT scheme, the collision term is defined in the following way (Bouarnouna *et al.* 2019, Shah *et al.* 2017):

$$\Omega_i = -M^{-1}C_i\left[m_i(x,t) - m_i^{eq}(x,t)\right] \tag{14}$$

where m_i and m_i^{eq} are macroscopic and equilibrium macroscopic variables, respectively.

4.1 D2Q9 MRT-LB Equation for the flow Field in Porous Media

For flow field, the two-dimensional nine velocities model D2Q9 is used in this study (Fig. 2). The MRT-LB equation (Higuera *et al.* 1989, Khali *et al.* 2013) with a specific treatment of the force term (Kumar *et al.* 2017, Li *et al.* 2010) is employed:

$$f_i(x+e_i\delta_t, t+\delta_t) - f_i(x,t) = -M^{-1}C_i\left[m_i(x,t) - m_i^{eq}(x,t)\right] + M^{-1}\delta_t\left(I - \frac{C_i}{2}\right)D_i \tag{15}$$

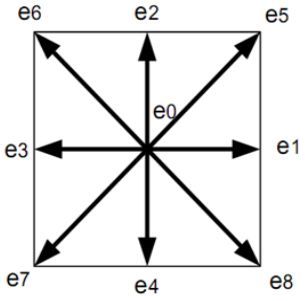

Fig. 2. The D2Q9 lattice structure.

The nine discrete velocities e_i are given by (Liu *et al.* 2014, Ghatreh Samani and Meghdadi Isfahani 2019):

$$e_i = \begin{cases} (0,0) & i = 0 \\ [\cos\phi, \sin\phi]c \quad \phi = (i-1)\dfrac{\pi}{2} & i = 1,2,3,4 \\ [\cos\phi, \sin\phi]\sqrt{2}c \quad \phi = (2i-9)\dfrac{\pi}{4} & i = 5,6,7,8 \end{cases} \tag{16}$$

where $c = (\delta_x/\delta_t) = (\delta_y/\delta_t)$ is the lattice speed, and δ_x and δ_y are the lattice cells dimensions, these quantities are chosen equal to the unit $\delta_x = \delta_y = \delta_t = 1$, thus $c = 1$.

The local equilibrium distribution function f_i^{eq} for the hydrodynamic field in porous medium is calculated by Eq. (17) (Fallah *et al.* 2012, Kumar *et al.* 2017):

$$f_i^{eq} = w_i\rho\left[1 + 3e_iv + \frac{9(e_iv)^2}{2\varepsilon} - \frac{3v^2}{2\varepsilon}\right] \tag{17}$$

where the weighting factors w_i are given as:

$$w_0 = 4/9\,;\; w_{1\text{-}4} = 1/9\,;\; w_{5\text{-}8} = 1/36 \tag{18}$$

M is the transformation matrix, which projects f_i and f_i^{eq} into the moment space via $m = Mf$ and $m^{eq} = Mf^{eq}$, in which m and m^{eq} are the macroscopic and equilibrium macroscopic variables vectors, respectively. The functions of distribution in moment space are described below (Fallah *et al.* 2012, Kumar *et al.* 2017):

$$m = \begin{pmatrix} \rho \\ e \\ \varphi \\ j_x - \frac{\delta_t}{2}\rho F_x \\ q_x \\ j_y - \frac{\delta_t}{2}\rho F_y \\ q_y \\ p_{xx} \\ p_{xy} \end{pmatrix} = \begin{bmatrix} 1 & 1 & 1 & 1 & 1 & 1 & 1 & 1 & 1 \\ -4 & -1 & -1 & -1 & -1 & 2 & 2 & 2 & 2 \\ 4 & -2 & -2 & -2 & -2 & 1 & 1 & 1 & 1 \\ 0 & 1 & 0 & -1 & 0 & 1 & -1 & -1 & 1 \\ 0 & -2 & 0 & 2 & 0 & 1 & -1 & -1 & 1 \\ 0 & 0 & 1 & 0 & -1 & 1 & 1 & -1 & -1 \\ 0 & 0 & -2 & 0 & 2 & 1 & 1 & -1 & -1 \\ 0 & 1 & -1 & 1 & -1 & 0 & 0 & 0 & 0 \\ 0 & 0 & 0 & 0 & 0 & 1 & -1 & 1 & -1 \end{bmatrix} \begin{pmatrix} f_0 \\ f_1 \\ f_2 \\ f_3 \\ f_4 \\ f_5 \\ f_6 \\ f_7 \\ f_8 \end{pmatrix} = Mf \tag{19}$$

where ρ is the fluid density, e is related to energy, φ is related to the square of the energy, $j_{x,y}$ are the momentum components $j = (j_x, j_y) = (\rho v_x, \rho v_y)$, $q_{x,y}$ are the energy flux in two directions, and $p_{xx,xy}$ refer to the diagonal and off-diagonal strain-rate tensor components.

Density ρ and momentum $j_{x,y}$ are conserved quantities, while the six other moments of velocity are non-conserved. m^{eq} for the non-conserved moments are described as (Liu *et al.* 2014):

$$\begin{aligned} e^{eq} &= -2\rho + \frac{3\rho_0|v|^2}{\varepsilon}\,;\; \varphi^{eq} = \rho - \frac{3\rho_0|v|^2}{\varepsilon}\,; \\ q_x^{eq} &= -\rho_0 v_x\,;\; q_y^{eq} = -\rho_0 v_y\,; \\ p_{xx}^{eq} &= \frac{\rho_0\left(v_x^2 - v_y^2\right)}{\varepsilon}\,;\; p_{xy}^{eq} = \frac{\rho_0 v_x v_y}{\varepsilon} \end{aligned} \tag{20}$$

In the equilibrium moments above, the incompressibility approximation was used. The fluid density is written in the following manner $\rho = (\rho_0 + \delta\rho) \approx \rho_0$ ($\delta\rho$ is the density fluctuation), and $j = (j_x, j_y) \approx \rho_0 v$. The mean fluid density ρ_0 is taken equal to 1 for simplicity.

I is the identity matrix and C is the diagonal relaxation matrix given by:

$$C = diag(s_0, s_1, s_2, s_3, s_4, s_5, s_6, s_7, s_8) \tag{21}$$

s_i are the relaxation rates. Their values must be between 0 and 2 to maintain stability. In this simulation, they are selected as follows:

$$C = diag(1, 1.2, 1.4, 1, 1.2, 1, 1.2, 1/\tau, 1/\tau) \tag{22}$$

The non-conserved moments relax in linear terms

into their equilibrium values (Mezrhab *et al.* 2010). In the moment space, the collision step is performed as:

$$m_i^*(x,t) = m_i(x,t) - C_i\left[m_i(x,t) - m_i^{eq}(x,t)\right] + \delta_t\left(I - \frac{C_i}{2}\right)D_i \quad (23)$$

In the velocity space, the streaming step is performed by:

$$f_i\ (x + e_i\delta_t, t + \delta_t) = f_i^*(x,t) \quad (24)$$

where $f^* = M^{-1}m^*$.

m^* is the moment after collision.

The constituents of the vector D in the moment space are as given below (Liu *et al.* 2014):

$$D_0 = 0\ ;\ D_1 = \frac{6\rho_0 vF}{\varepsilon}\ ;\ D_2 = -\frac{6\rho_0 vF}{\varepsilon}\ ;\ D_3 = \rho_0 F_x\ ;$$
$$D_4 = -\rho_0 F_x\ ;\ D_5 = \rho_0 F_y\ ;\ D_6 = -\rho_0 F_y\ ; \quad (25)$$
$$D_7 = \frac{2\rho_0\left(v_x F_x - v_y F_y\right)}{\varepsilon}\ ;\ D_8 = \frac{\rho_0\left(v_x F_y + v_y F_x\right)}{\varepsilon}$$

In the MRT-LBM, the fluid kinematic viscosity is related to the relaxation parameter of the flow field τ (Guo *et al.* 2010):

$$\upsilon = \frac{1}{3}\left(\tau - \frac{1}{2}\right) \quad (26)$$

For a Newtonian fluid, τ is constant in each node, whereas for a power law fluid, τ is variable according to the local strain rate (Sullivan *et al.* 2006). The form of local viscosity for the power law fluid is given by:

$$\upsilon = K'\left(\dot{\gamma}\right)^{n-1} \quad (27)$$

$\dot{\gamma}$ is the local shear rate. It is linked to the symmetrical strain rate tensor's second invariant $S_{\alpha'\beta'}$ in the following way (Sullivan *et al.* 2006):

$$\dot{\gamma} = 2\sqrt{S_{\alpha'\beta'}S_{\alpha'\beta'}} \quad (28)$$

with

$$S_{\alpha'\beta'} = \frac{\partial v_{\alpha'}}{\partial x_{\beta'}} + \frac{\partial v_{\beta'}}{\partial x_{\alpha'}} \quad (29)$$

In MRT method, the strain rate tensor $S_{\alpha'\beta'}$ may be written as (Fallah *et al.* 2012):

$$S_{\alpha'\beta'} = -\frac{1}{2\rho C_S^2\delta_t}\sum_{j=0}^{8} e_{j\alpha'}e_{j\beta'}\sum_{i=0}^{8}\left(M^{-1}SM\right)_{ji}\left[f_i(x,t) - f_i^{eq}(x,t)\right] \quad (30)$$

where $C_S = c/\sqrt{3}$ is the speed of sound.

The macroscopic fluid variables are calculated as follows:

$$\rho = \sum_{i=0}^{8} f_i \quad (31)$$

$$\rho_0 v = \sum_{i=0}^{8} e_i f_i + \frac{\delta_t}{2}\rho_0 F \quad (32)$$

4.2 D2Q5 MRT-LB Equation for the Temperature Field

The two-dimensional D2Q5 model (Fig. 3) with five velocities is used in this work for the temperature field. The MRT-LB equation may be written as:

$$g_i(x + e_i\delta_t, t + \delta_t) - g_i(x,t) = -N^{-1}E_i\left[n_i(x,t) - n_i^{eq}(x,t)\right] \quad (33)$$

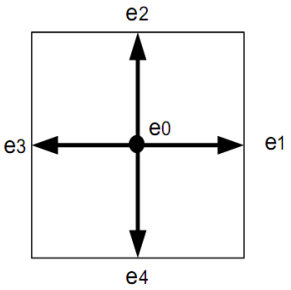

Fig. 3. The D2Q5 lattice structure.

where $g_i(x,t)$ is the function of temperature distribution.

In D2Q5 model, e_i are given by:

$$e_i = \begin{cases} (0,0) & i = 0 \\ \left[\cos\phi, \sin\phi\right]c \quad \phi = (i-1)\dfrac{\pi}{2} & i = 1,2,3,4 \end{cases} \quad (34)$$

The function of equilibrium distribution is denoted by:

$$g_i^{eq} = w_i T\left[1 + 5e_i v\right] \quad (35)$$

where the weighting factors w_i' are given as:

$$w_0' = 3/5\ ;\ w_{1-4}' = 1/10 \quad (36)$$

N is the 5×5 orthogonal transformation matrix, which projects g_i and g_i^{eq} into the moment space with $n = Ng$ and $n^{eq} = Ng^{eq}$, where n and n^{eq} are the macroscopic and equilibrium macroscopic temperature variables, respectively.

The functions of temperature distribution in moment space are provided below (Mezrhab *et al.* 2010):

$$n = \begin{pmatrix} n_0 \\ n_1 \\ n_2 \\ n_3 \\ n_4 \end{pmatrix} = \begin{bmatrix} 1 & 1 & 1 & 1 & 1 \\ 0 & 1 & 0 & -1 & 0 \\ 0 & 0 & 1 & 0 & -1 \\ -4 & 1 & 1 & 1 & 1 \\ 0 & 1 & -1 & 1 & -1 \end{bmatrix} \begin{pmatrix} g_0 \\ g_1 \\ g_2 \\ g_3 \\ g_4 \end{pmatrix} = Ng \quad (37)$$

E is the diagonal relaxation matrix:

$$E = diag\left(r_0, r_1, r_2, r_3, r_4\right) \quad (38)$$

Table 1 Comparison of average Nusselt number for various Da and Ra. $\varepsilon = 0.4$; Pr = 1

Da	Ra	Liu *et al.* (2014)	Nithiarasu *et al.* (1997)	Guo and Zhao (2005)	Present work	Maximum relative deviation (%)
10^{-2}	10^3	1.007	1.010	1.008	1.008	0,198
	10^4	1.362	1.408	1.367	1.357	3,622
	10^5	3.009	2.983	2.998	3.057	2,480
10^{-4}	10^5	1.067	1.067	1.066	1.066	0,093
	10^6	2.630	2.550	2.603	2.597	1,843
	10^7	7.808	7.810	7.788	7.792	0,230
10^{-6}	10^7	1.085	1.079	1.077	1.077	0,737
	10^8	2.949	2.970	2.955	2.935	1,178
	10^9	11.610	11.460	11.395	11.770	3,290

For stability reasons, the relaxation rates are chosen as follows:

$$E = diag(1,1/\tau_T,1/\tau_T,1.25,1.25) \tag{39}$$

where τ_T is the relaxation parameter for temperature field.

The D2Q5 MRT-LB collision process is accomplished as follows:

$$n_i^*(x,t) = n_i(x,t) - E\left[n_i(x,t) - n_i^{eq}(x,t)\right] \tag{40}$$

Among the 5 moments, only temperature is conserved:

$$n_0 = T = \sum_{i=0}^{4} g_i \tag{41}$$

The non-conserved moments are written in equilibrium as follows: (Lallemand *et al.* 2003)

$$n_1^{eq} = v_x T \; ; \; n_2^{eq} = v_y T \; ; \; n_3^{eq} = \varpi T \; ; \; n_4^{eq} = 0 \tag{42}$$

The effective thermal diffusivity α_e is defined as:

$$\alpha_e = \frac{\sigma(4+\varpi)}{10}\left(\tau_T - \frac{1}{2}\right) \tag{43}$$

The thermal transfer between the hot cavity wall and the cold fluid is characterized by the local (Nu) and the mean (Nu_{avg}) Nusselt numbers:

$$\mathrm{Nu} = -\left.\frac{\partial T}{\partial y}\right|_{y=0} \quad \text{and} \quad \mathrm{Nu}_{avg} = \int_0^1 \mathrm{Nu}\, dx \tag{44}$$

4.3 Boundary Conditions

In the LBM, conditions should be introduced through the distribution function.

Boundary conditions for flow:

Bounce Back conditions are employed for specifying boundary conditions on the solid walls. The distribution functions at the solid are equal to the distribution functions of the fluid (Rahmati and Najjarnezami 2016). For the D2Q9 model:

upper wall:

$$f_{4,n} = f_{2,n} \;,\; f_{7,n} = f_{5,n} \;,\; f_{8,n} = f_{6,n} \tag{45}$$

lower wall:

$$f_{2,n} = f_{4,n} \;,\; f_{5,n} = f_{7,n} \;,\; f_{6,n} = f_{8,n} \tag{46}$$

left wall:

$$f_{1,n} = f_{3,n} \;,\; f_{5,n} = f_{7,n} \;,\; f_{8,n} = f_{6,n} \tag{47}$$

right wall:

$$f_{3,n} = f_{1,n} \;,\; f_{7,n} = f_{5,n} \;,\; f_{6,n} = f_{8,n} \tag{48}$$

Boundary conditions for Temperature:

For the thermal field (D2Q5 model):

The Bounce Back condition is also used on the adiabatic walls:

upper wall:

$$g_{2,n} = g_{2,n-1} \tag{49}$$

lower isolated portions:

$$g_{4,n} = g_{4,n-1} \tag{50}$$

and in the isothermal walls, we applied in the:

left wall:

$$g_1 = 2\left(\frac{1}{5} + \frac{\varpi}{20}\right)T_C - g_3 \tag{51}$$

right wall:

$$g_3 = 2\left(\frac{1}{5} + \frac{\varpi}{20}\right)T_C - g_1 \tag{52}$$

lower heated portion:

$$g_2 = 2\left(\frac{1}{5} + \frac{\varpi}{20}\right)T_H - g_4 \tag{53}$$

5. Code Validation And Mesh Sensitivity Analysis

The computational code has been successfully approved with the numerical works of Liu *et al.* (2014), Nithiarasu *et al.* (1997) and Guo and Zhao (2005), for the case of differentially heated porous cavity with isolated horizontal walls. This cavity of porosity equal to 0.4 is filled with a Newtonian fluid. Table 1 indicates a good accordance between the average Nusselt numbers obtained from this code and those of the mentioned papers, for different Darcy and Rayleigh numbers, with a

Table 2 Grid independence study for n = 0.7, 1 and 1.3. Ra = 10^4; Da = 10^{-3}; R = 0.3.

	n = 0.7		n = 1		n = 1.3	
Grid	Nu_{avg}	Relative gap (%)	Nu_{avg}	Rela-tivegap (%)	Nu_{avg}	Relative gap (%)
80×80	4.7666	-	4.1222	-	3.8385	-
100×100	4.7880	0.448	4.1347	0.303	3.8499	0.297
120×120	4.8048	0.351	4.1441	0.227	3.8560	0.158
140×140	4.8115	0.139	4.1488	0.113	3.8575	0.039
160×160	4.8119	0.008	4.1499	0.026	3.8582	0.018
180×180	4.8125	0.012	4.1505	0.014	3.8586	0.010
200×200	4.8126	0.002	4.1505	0.000	3.8587	0.003

maximum relative deviation of about 3.62 %. The values were compared with the three works and the maximum relative deviation is reported.

The code is also validated with the numerical work of Turan *et al.* (2011) in the case of differentially heated cavity filled by a power law fluid. Figure 4 shows a good correspondence between isotherms obtained from this code and those of Turan *et al.* (2011), for several power law indices and Numbers of Rayleigh.

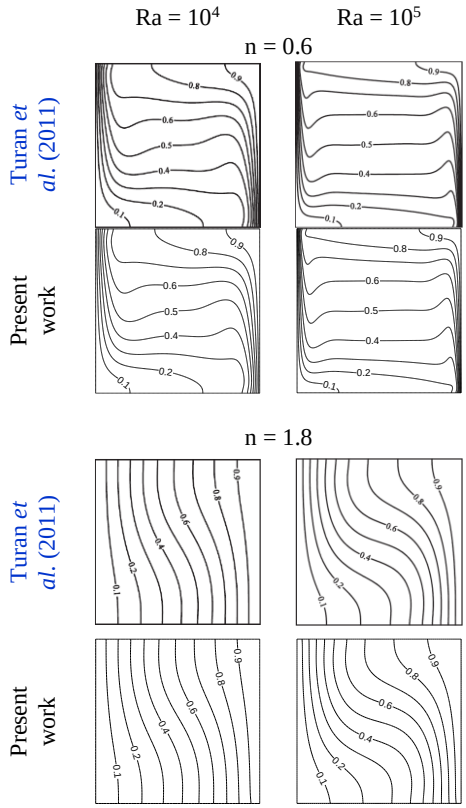

Fig. 4. Comparison of isotherms with those of Turan *et al.* (2011).

Before tackling the simulations results, the mesh sensitivity analysis was performed to assure a grid independent solution. The Mesh influence on the mean Nusselt number of the hot horizontal wall is shown on Table 2 for various power law indices, with Ra = 10^4, Da = 10^{-3} and R = 0.3. The relative gap of the average Nusselt number of each mesh, compared to the result of the prior mesh, is presented. Based on the simulation runs, the uniform mesh size of 180×180 nodes was selected for the rest of the simulations.

6. OUTCOMES WITH EXPLANATIONS

This study is performed primarily to exhibit the applicability of the MRT-LBM method and its simplicity of implementation, compared to more classical methods. The analysis was, therefore, restricted to the treatment of the effect of certain parameters, namely: power law index, Rayleigh number, Darcy number and the radius ratio of the porous deposit, on hydrodynamic and heat transfer. The power law index ranges from 0.6 to 1.4, the Rayleigh number varies between 10^3 and 10^6, Darcy number takes its values between 10^{-5} and 10^{-2} and the radius ratio of the porous deposit is chosen between 0.05 and 0.5.

In the simulations below, the necessary parameters are fixed at these values: Pr = 10, ε = 0.6, α_e / α = 1 (α is the fluid's thermal diffusivity), J = 1 and $\varpi = -2$.

To respect the incompressible flow approximation and the stability criterion on υ, the Mach number based on U (Ma = U / C_S) should be less than 0.3. $U = \sqrt{g \beta \Delta T L}$ is the characteristic velocity in thermal convective flows.

Figure 5 presents the influence of power law index on streamlines for multiple Rayleigh numbers with Da = 10^{-3} and R = 0.3. For the elevated numbers of Rayleigh (Ra = 10^6), the structure of streamlines shows that the natural convection transport becomes stronger for the pseudoplastic fluid compared to the dilatant one. However, the low buoyancy forces in the lower Rayleigh numbers significantly slow the movement of the fluid and the flow pattern becomes almost independent of n. Therefore, the effects of shear-thinning and shear-thickening appear insignificant except inside the porous medium, where the flux of the pseudoplastic fluid is weaker as compared to the Newtonian and dilatant fluids. This is due to the lightness of this fluid that is deflected by the porous deposit.

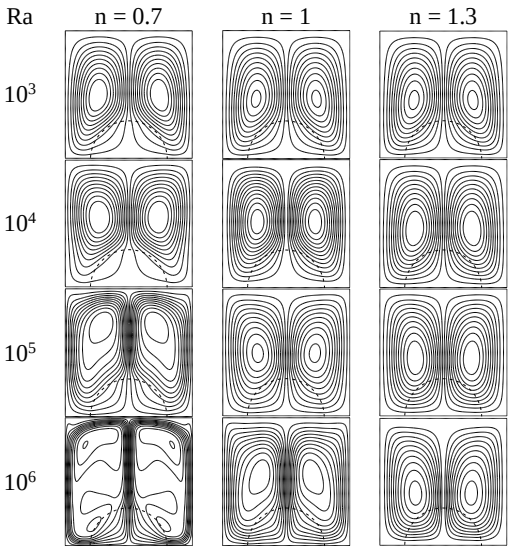

Fig. 5. Streamlines for various power law indices and Rayleigh numbers. Da = 10^{-3} ; R = 0.3.

The effect of power law index on isotherms for several Rayleigh numbers at Da = 10^{-3} and R = 0.3 is presented on Fig. 6. For the smallest Rayleigh numbers (Ra = 10^3), it can be observed that isotherms are similar for all three types of power law fluid and the conduction is dominant, given the low intensity of convective currents. However, for larger Rayleigh numbers, the thermal transfer becomes more convective and the decrease in power law index reduces the thermal boundary layer thickness near the walls. This is due to the low apparent viscosity that improves thermal transfer, referring to the increase in the rate of parietal gradients. It is of interest to note that the cold fluid follows the vertical walls in a downward movement, in the form of two concentric cells, given the high density, and then rises through the centre forming a thermal plume.

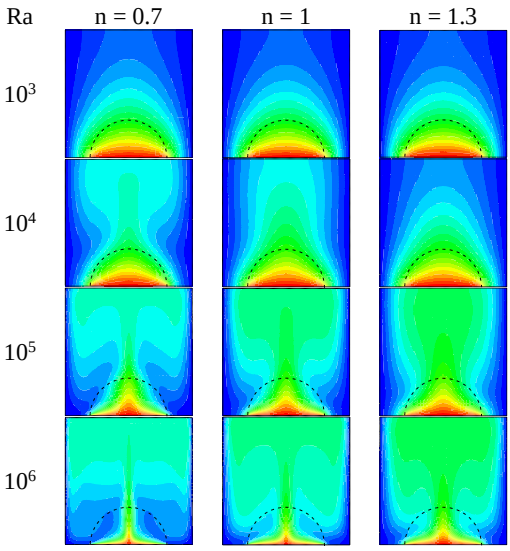

Fig. 6. Isotherms for various power law indices and Rayleigh numbers. Da = 10^{-3}; R = 0.3.

The impact of varying the power law index and Darcy number on flow field is also investigated. Results are illustrated in Fig. 7 for Ra = 10^5 and R = 0.3. At higher numbers of Darcy (Da = 10^{-3} and 10^{-2}), the flow is able to penetrate more deeply inside the porous deposit without disturbance for pseudoplastic, Newtonian and dilatant fluids because of the high permeability. Nevertheless, the convective flow in porous matrix is weak for lower Darcy numbers (Da = 10^{-5} and 10^{-4}), given that the deposit becomes quasi-solid and causes deflection of streamlines. But even so, the extremely external streamlines, induced by the strong convective currents existing at the vertical walls, are only able to penetrate the porous deposit.

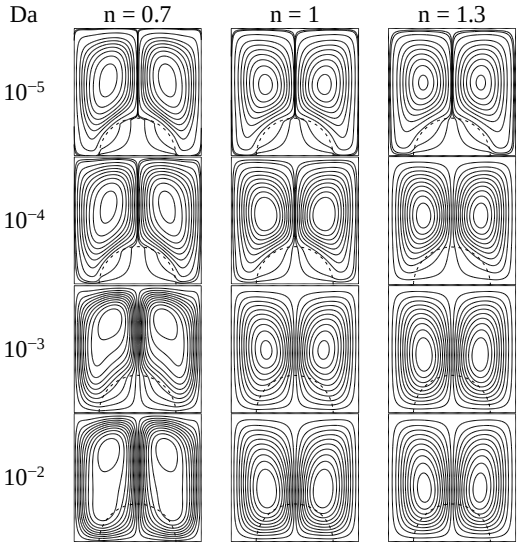

Fig. 7. Streamlines for various power law indices and Darcy numbers. Ra = 10^5; R = 0.3.

Figure 8 displays isotherms for different power law indices and Darcy numbers with Ra = 10^5 and R = 0.3. Clearly, improving the Darcy number reduces significantly the thickness of the thermal plume and boundary layer for the pseudoplastic fluid. For Da = 10^{-5} and Da = 10^{-4}, the conduction heat transfer is dominant within the porous deposit for the three considered fluids. In particular, for the pseudoplastic fluid, the cold fluid descending along the vertical walls goes around the porous deposit. This phenomenon is attenuated when dealing with the dilatant fluid given the magnitude of the apparent viscosity. Therefore, in the case of pseudoplastic fluid, the hot fluid inside the deposit is prevented from invading the upper regions of the cavity and only a plume of hot fluid is observed. This is not the case for the dilatant fluid where the cold fluid is less reassembled and thus allows the expansion of the hot fluid.

Figure 9 reveals the effect of power law index and Darcy number on the average Nusselt number, calculated on the hot portion of the bottom wall for Ra = 10^5 and R = 0.3. Note that the heat transfer rate decreases with the increase of power law index. The previous behaviour is owed to the fact that the augmentation of n leads to an enhancement in the effective viscosity which reduces convective currents in the cavity. Moreover, the heat transfer

rate rises sharply with the increase of Da, in particular in the case of pseudoplastic fluid. This derives from the reduction in the hydraulic resistance of the porous matrix. In this manner, the fluid circulation and the heat transfer are thereby increased. When the Darcy number is equal to 10^{-5} and 10^{-4}, it is noticed that n influences slightly the heat transfer rate. On the other hand, as Da increases from 10^{-4} to 10^{-3}, the impact of n becomes more prominent. For Da = 10^{-2} the heat transfer rate decreases more sharply with the increase of n.

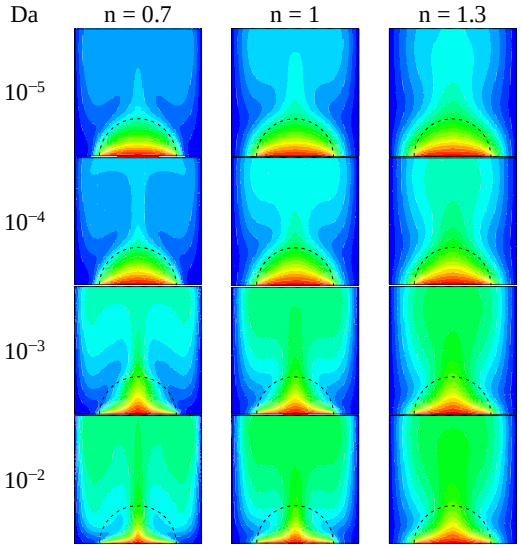

Fig. 8. Isotherms for various power law indices and Darcy numbers. Ra = 10^5 ; R = 0.3.

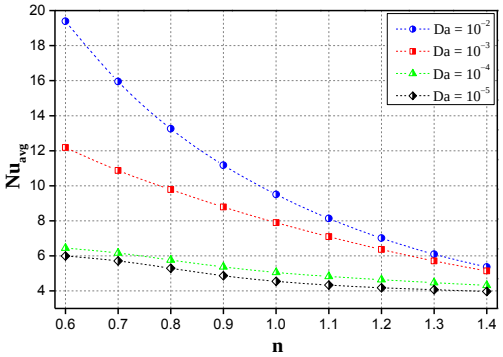

Fig. 9. Effect of power law index for various Darcy numbers on average Nusselt number. Ra = 10^5; R = 0.3.

Figure 10 demonstrates the effect of Rayleigh number for different power law indices on the heat transfer rate when Da = 10^{-5} and 10^{-3} and R = 0.3. Obviously, the mean Nusselt number rises with the rise in the number of Rayleigh. For $10^3 \leq Ra \leq 10^4$, n has a small impact on the rateof heat transfer. This may be attributed to the slow movement of the fluid caused by the low buoyancy forces and thus the effects of shear-thinning and shear-thickening did not appear significantly. Above Ra = 10^4, the heat transfer rate is enhanced significantly by increasing n, especially in the case of Da = 10^{-3}. It can be explained by the improvement of the convective transport.

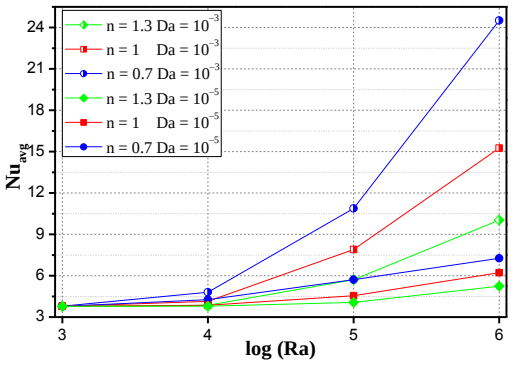

Fig. 10. Effect of Rayleigh number for various power law indices on average Nusselt number. Da = 10^{-5} and Da = 10^{-3} ; R = 0.3.

The influence of radius ratio, of the semi-cylindrical porous deposit, and Darcy number on the mean Nusselt number with n = 0.7 and 1.3 is shown in Fig. 11 and Fig. 12, respectively. Since the hot partition is in a larger contact with the fluid for the lowest radius ratios, the average Nusselt number becomes higher. The rate of heat transfer is less important for lower values of Darcy number, because the porous deposit behaves like a solid and therefor presents an important hydrodynamic resistance. Then, the reduction of its radius reduces this resistance, which is less important in the high Darcy numbers.

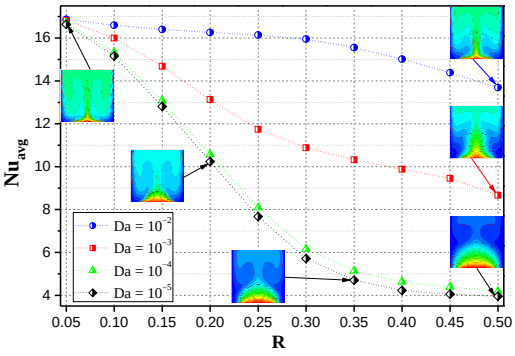

Fig. 11. Effect of radius ratio for various Darcy numbers on average Nusselt number. n = 0.7 ; Ra = 10^5.

Figure 13 illustrates the effect of radius ratio for different power law indices on the mean Nusselt number with Da = 10^{-4} and Ra = 10^4. The mean number of Nusselt decreases sharply with the increase in radius ratio for the pseudoplastic fluid, while it decreases slightly for the Newtonian one, and in particular for the dilatant fluid, where an independence of the Nusselt number according to R is noted. By observing those curves closely, an unusual behaviour is noticed for the pseudoplastic and Newtonian fluids, which offer the same transfer rate as the dilatant fluid for radius ratio greater than 0.4. A more careful observation of the isotherms corresponding to these cases shows that for the

pseudoplastic case, the descending currents along the cold vertical walls come to bypass the porous deposit (less permeable: Da = 10^{-4}) and confine the hot fluid to the lower (hot) wall. Then, the heat is only evacuated by a central restricted region. Furthermore, for the dilatant fluid, the heat is only prevented in its upward ascent by the value of the apparent viscosity. In the case of pseudoplastic and Newtonian fluids, this upward ascent is hindered by this cold fluid cover, which settles above the porous deposit and hence the hot fluid cannot cross or bypass.

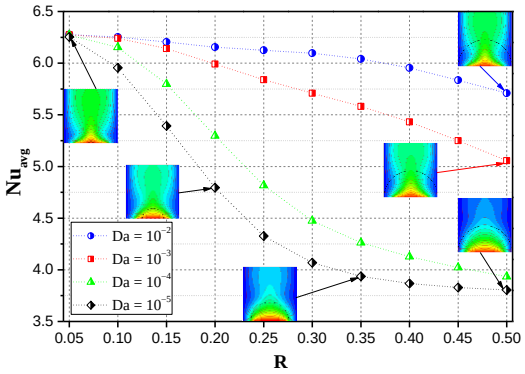

Fig. 12. Effect of radius ratio for various Darcy numbers on average Nusselt number.n = 1.3 ; Ra = 10^5.

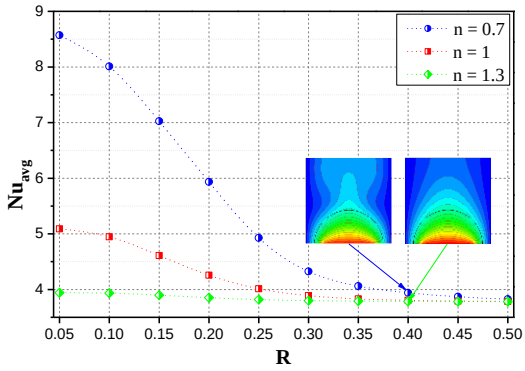

Fig. 13. Effect of radius ratio for various power law indices on average Nusselt number. Da = 10^{-4} ; Ra = 10^4.

Figure 14 exposes the local temperature at Y = 0.5 for various power law indices and Rayleigh numbers with R = 0.3, Da = 10^{-5} and Da = 10^{-2}. For each Rayleigh number, the increase in Darcy number from 10^{-5} to 10^{-2} shows a noticeable impact on the temperature profile. This is attributed to the increased role of convection on the heat transport inside the cavity as the permeability improves. For Ra = 10^3, Similar temperature profiles are obtained with all three types of fluid for Da = 10^{-5}. However, for Da = 10^{-2}, the local temperature increases by decreasing the power law index. This is attributed to the decrease in apparent viscosity. For Ra = 10^4, the local temperature of Newtonian fluid becomes superior to that of the pseudoplastic. This is attributed to the strong currents of cold fluid flowing down along the vertical walls that reduce the temperature in the case of pseudoplastic fluid. When Rayleigh increases to 10^5 and 10^6, the temperature profiles are reversed in the part away from the cold walls and the dilatant fluid offers the highest temperature in this part. This can be explained by the fact that when buoyancy forces rise through the increase in Rayleigh number, the descending currents along the cold vertical walls confine the hot fluid to the lower wall. Therefore, the fluid with the highest apparent viscosity displays the highest temperature values at the cavity centre. On the other hand, the parietal (horizontal) temperature gradients are more important for the pseudoplastic fluid compared to the dilatant one, except in the case of Ra = 10^6 and Da = 10^{-5}, where the gradients are essentially similar.

7. CONCLUSION

Through this paper, numerical simulation of natural convection of power law fluid within a partially heated square cavity, with a porous deposit, were performed by employing a home made code. The code is based on MRT-LBM. Thereby, the effects of the pertinent parameters, including power-law index, number of Darcy, number of Rayleigh and the radius of the semi-cylindrical porous deposit, on hydrodynamic and heat transfer were extensively examined. The resulting predictions produced the conclusions as follows:

- The good consistency with previous predictions indicates the suitability of the used MRT-LBM model with this kind of industrial problems.
- The increase in the numbers of Rayleigh and Darcy and the decrease in the power law index, increase convective flow in the cavity and enhance the heat transfer rate.
- For lower Darcy numbers, the descending currents of pseudoplastic fluid along the cold vertical walls come to bypass the porous deposit and confine the hot fluid on the lower wall. The heat is then only evacuated by a central restricted region which is as low as n is small.
- The average number of Nusselt is higher for the lowest radius ratios of the semi-cylindrical porous deposit, and the improvement in the Darcy number enhances the thermal transfer rate especially for pseudoplastic fluid.
- For a porous deposit radius ratio greater than 0.4, the pseudoplastic and Newtonian fluids have similar heat transfer rates to that of the dilatant fluid in the case of low permeability.
- An unusual phenomenon is noticed for high Rayleigh numbers, where better heat evacuation from the porous deposit is noticed for the dilatant fluid compared to the pseudoplastic one.

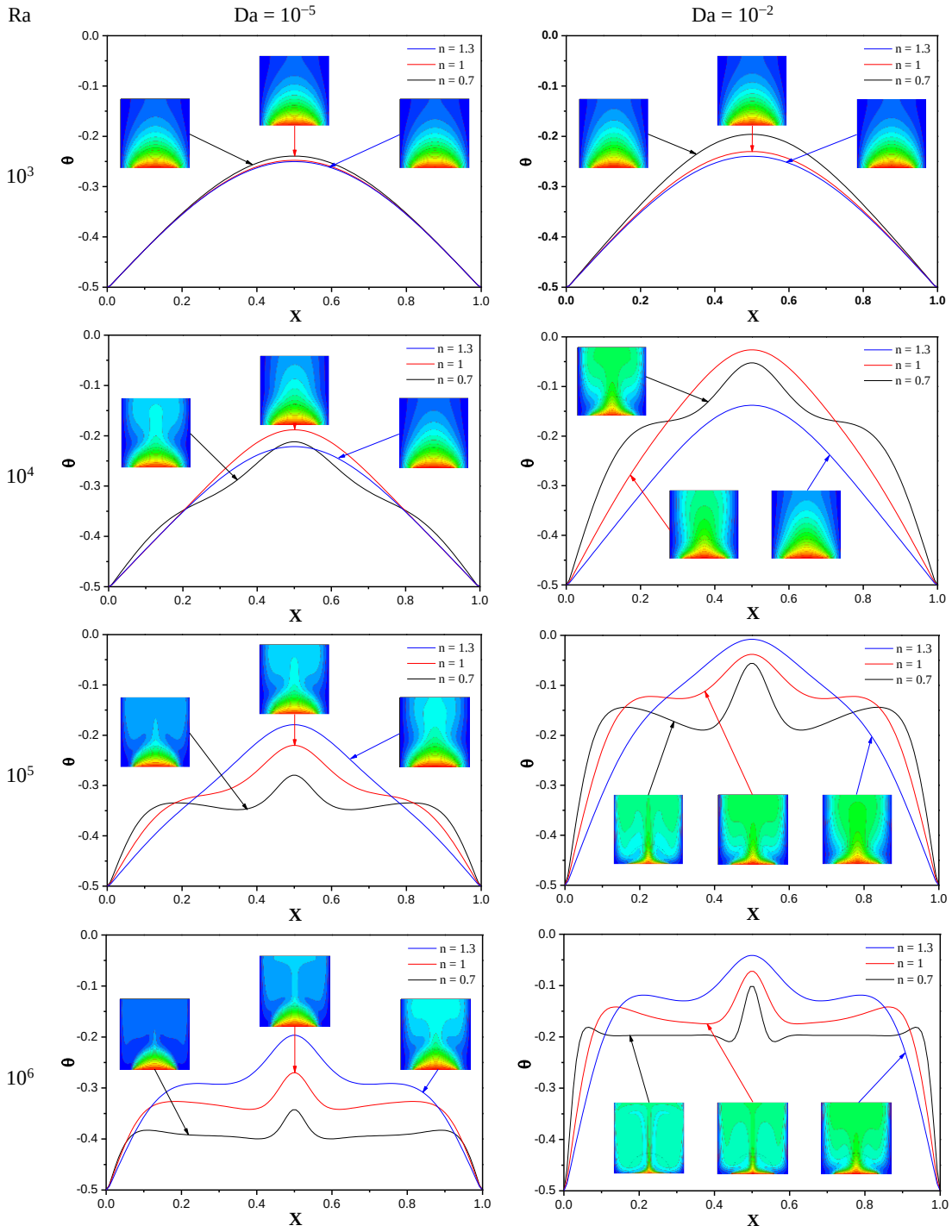

Fig. 14. Temperature distribution at Y = 0.5 for different power law indices and Rayleigh numbers. Da = 10^{-5} and Da = 10^{-2} ; R = 0.3.

REFERENCES

Abdel-gaied, S. M. and M. R. Eid (2011). Natural convection of non-Newtonian power-law fluid over axisymmetric and two-dimensional bodies of arbitrary shape in fluid-saturated porous media. *Applied Mathematics and Mechanics (English Edition)* 32(2), 179-188.

Astanina, M. S., M. A. Sheremet and J. C. Umavathi (2018). Transient natural convection with temperature-dependent viscosity in a square partially porous cavity having a heat-generating source. *Numerical Heat Transfer, Part A: Applications* 73(12), 849-862.

Basak, T., S. Roy, T. Paul and I. Pop (2006). Natural convection in a square cavity filled

with a porous medium: Effects of various thermal boundary conditions. *International Journal of Heat and Mass Transfer* 49(7–8), 1430-1441.

Bejan, A. (2004). *Convection Heat Transfer*. Wiley, New Jersey, USA.

Bhatnagar, P. L., E. P. Gross and M. Krook (1954). A model for collision processes in gases. I. Small amplitude processes in charged and neutral one-component systems. *Physical Review* 94(3), 511-525.

Bouarnouna, K., A. Boutra, K. Ragui, N. Labsi and Y. K. Benkahla (2019). Multiple-relaxation-time lattice Boltzmann model for flow and convective heat transfer in channel with porous media. *Journal of Statistical Physics* 174(5), 970-991.

Boutra, A., Y. K. Benkahla, D. E. Ameziani and R. Bennacer (2017). lattice Boltzmann simulation of natural convection in cubical enclosures for the Bingham plastic fluid. *Heat Transfer Research* 48(7), 607-624.

Chen, X. B., P. Yu, Y. Sui, S. H. Winoto and H. T. Low (2009). Natural convection in a cavity filled with porous layers on the top and bottom walls. *Transport in Porous Media* 78(2), 259-276.

Christopher, R. H. and S. Middleman (1965). Power-law flow through a packed tube. *Industrial & Engineering Chemistry Fundamentals* 4(4), 422-426.

D'Humières, D. (1992). Generalized lattice Boltzmann equations. *The American Institute of Aeronautics and Astronautics* 159, 450-458.

Dash, S. M. and T. S. Lee (2014). Natural convection from inclined square cylinder using novel flexible forcing IB-LBM approach. *Engineering Applications of Computational Fluid Mechanics* 8(1), 91-103.

Dash, S. M. and T. S. Lee (2015). Natural convection in a square enclosure with a square heat source at different horizontal and diagonal eccentricities. *Numerical Heat Transfer, Part A* 68(6), 686-710.

Dash, S. M., T. S. Lee and H. Huang (2014). Natural convection from an eccentric square cylinder using a novel flexible forcing IB-LBM method. *Numerical Heat Transfer, Part A* 65(6), 531-555.

Dharmadhikari, R. V. and D. D. Kale (1985). Flow of non-Newtonian fluids through porous media. *Chemicd Engineering Science* 40(3), 527-529.

Fallah, K., M. Khayat, M. H. Borghei, A. Ghaderi and E. Fattahi (2012). Multiple-relaxation-time lattice Boltzmann simulation of non-Newtonian flows past a rotating circular cylinder. *Journal of Non-Newtonian Fluid Mechanic*s 177(Apr.), 1-14.

Gangawane, K. M. and B. Manikandan (2017). Laminar natural convection characteristics in an enclosure with heated hexagonal block for non-Newtonian power law fluids. *Chinese Journal of Chemical Engineering* 25(5), 555-571.

Getachew, D., W. J. Minkowycz and D. Poulikakost (1996). Natural convection in a porous cavity saturated with a non-Newtonian fluid, *Journal of Thermophysics and Heat Transfer* 10(4), 640-651.

Ghatreh Samani, S. and A. H. Meghdadi Isfahani (2019). A new relaxation time model for lattice Boltzmann simulation of nano couette flows in wide range of flow regimes. *Journal of Applied Fluid Mechanics* 12(6), 1781-1790.

Guo, Y., R. Bennacer, S. Shen, D. E. Ameziani and M. Bouzidi (2010). Simulation of mixed convection in slender rectangular cavity with Lattice-Boltzmann method. *International Journal of Numerical Methods for Heat & Fluid Flow* 20(1), 130-148.

Guo, Z. and T. S. Zhao (2005). A lattice Boltzmann model for convection heat transfer in Porous media. *Numerical Heat Transfer Part B: Fundamentals* 47(2), 157-177.

Habbachi, F., F. S. Oueslati, R. Bennacer, M. Ganaoui and A. Elcafsia (2017). Three-dimensional simulation of natural convection in cubic cavity partially filled with porous media. *Energy Procedia* 139, 617-623.

Habibi Matin, M., I. Pop and S. Khanchezar (2013). Natural convection of power-law fluid between two-square eccentric duct annuli. *Journal of Non-Newtonian Fluid Mechanics* 197(Feb.), 11-23.

Heidary, H., M. J. Kermani and M. Pirmohammadi (2016). Partition effect on thermo magnetic natural convection and entropy generation in inclined porous cavity. *Journal of Applied Fluid Mechanics* 9(1), 119-130.

Higuera, F. J., S. Succi and R. Benzi (1989). Lattice gas dynamics with enhanced collisions. *Europhysics Letters* 9(4), 345-349.

Jafari, Y., M. Taeibi-Rahni, M. Haghshenas and P. Ramian (2018). Lattice Boltzmann numerical investigation of inner cylindrical pin-fins configuration on nanofluid natural convective heat transfer in porous enclosure. *Journal of Applied Fluid Mechanics* 11(3), 801-816.

Jecl, R. and L. Skerget (2003). Boundary element method for natural convection in non-Newtonian fluid saturated square porous cavity. *Engineering Analysis with Boundary Elements* 27(10), 963-975.

Kefayati, G. H. R. (2016). Simulation of double diffusive natural convection and entropy generation of power-law fluids in an inclined porous cavity with Soret and Dufour effects (Part I: Study of fluid flow, heat and mass

transfer). *International Journal of Heat and Mass Transfer* 94(Dec.), 539-581.

Kemblowski, Z. and M. Michniewicz (1979). A new look at the laminar flow of power-law fluids through granular beds. *Rheologica Acta* 18(6), 730-739.

Khali, S., R. Nebbali, K. Bouhadef and D. E. Ameziani (2013). Numerical investigation of non-Newtonian fluids in annular ducts with finite aspect ratio using lattice Boltzmann method. *Physical Review E* 87(5), 053002.

Khezzar, L., D. Siginer and I. Vinogradov (2012). Natural convection of power law fluids in inclined cavities. *International Journal of Thermal Sciences* 53(Dec.), 8-17.

Kumar, C. S., S. Mohankumar, M. Geier and A. Pattamatta (2017). Numerical investigations on convective heat transfer enhancement in jet impingement due to the presence of porous media using Cascaded Lattice Boltzmann method. *International Journal of Thermal Sciences* 122(Aug.), 201-217.

Lallemand, P. and L. S. Luo (2003). Theory of the lattice Boltzmann method: acoustic and thermal properties in two and three dimensions. *Physical Review E* 63(3) 036706

Li, Q., Y. L. He, G. H. Tang and W. Q. Tao (2010). Improved axisymmetric lattice Boltzmann scheme, *Physical Review E* 81(5), 056707.

Liu, Q., Y. L. He, Q. Li and W.Q. Tao (2014). A multiple-relaxation-time lattice Boltzmann model for convection heat transfer in porous media. *International Journal of Heat Mass Transfer* 73(Feb.), 761-775.

Mezrhab, A., M. A. Moussaoui, M. Jami, H. Naji, and M. H. Bouzidi (2010). Double MRT thermal lattice Boltzmann method for simulating convective flows. *Physics Letters A* 374(34), 3499-3507.

Nebbali, R. and K. Bouhadef (2011). Non-Newtonian fluid flow in plane channels: Heat transfer enhancement using porous blocks. *International Journal of Thermal Sciences* 50(10), 1984-1995.

Nithiarasu, P., K. N. Seetharamu and T. Sundararajan (1997). Natural convective heat transfer in a fluid saturated variable porosity medium. *International Journal of Heat and Mass Transfer* 40(16), 3955-3967.

Omara, A., A. Bourouis and S. Abboudi (2016). Numerical approach of thermal non equilibrium natural convection in a square porous cavity with partially thermally active side walls. *Journal of Applied Fluid Mechanics* 9(2), 223-233.

Ragui, K., A. Boutra, R. Bennacer and Y. K. Benkahla (2017). Critical dimension of a circular heat and solute source for an optimum transfer within square porous enclosures. *Energy Procedia* 139, 817-823.

Rahmati, A. R. and A. Najjarnezami (2016). A double multi-relaxation-time lattice Boltzmann method for simulation of magneto hydrodynamics. *Journal of Applied Fluid Mechanics* 9(3), 1201-1214.

Raizah Abdelraheem, Z. A. S., M. Aly and S. E. Ahmed (2018). Natural convection flow of a power-law non-Newtonian nanofluid in inclined open shallow cavities filled with porous media. *International Journal of Mechanical Sciences* 140(Mar.), 376-393.

Shah, N., P. Dhar, S. K. Chinige, M. Geier and A. Pattamatta (2017). Cascaded collision lattice Boltzmann model (CLBM) for simulating fluid and heat transport in porous media. *Numerical Heat Transfer, Part B: Fundamentals* 72(3), 211-232.

Shenoy, A. V. (1994). Non-Newtonian fluid heat transfer in porous media. *Advances in Heat Transfer* 24, 101-190.

Sullivan, S. P., L. F. Gladden and M. L. Johns (2006). Simulation of power-law fluid flow through porous media using lattice Boltzmann techniques. *Journal of Non-Newtonian Fluid Mechanics* 133(2-3), 91-98.

Turan, O., A. Sachdeva, N. Chakraborty and R. J. Poole (2011). Laminar natural convection of power-law fluids in a square enclosure with differentially heated side walls subjected to constant temperatures. *Journal of Non-Newtonian Fluid Mechanics* 166(17-18), 1049-1063.

Zhuang, Y. J. and Q. Y. Zhu (2018). Numerical study on combined buoyancy–Marangoni convection heat and mass transfer of power-law nanofluids in a cubic cavity filled with a heterogeneous porous medium. *International Journal of Heat and Fluid Flow* 71(Mar.), 39-54.

Zhuang, Y. J., H. Z. Yu and Q. Y. Zhu (2017). A thermal non-equilibrium model for 3D double diffusive convection of power-law fluids with chemical reaction in the porous medium. *Intenational. Journal of Heat Mass Transfer* 115(Aug.), 670-694.